Journal of Neuroscience Methods 186 (2010) 116–129

Contents lists available at ScienceDirect

Journal of Neuroscience Methods

journal homepage: www.elsevier.com/locate/jneumeth

Revealing neuronal functional organization through the relation between multi-scale oscillatory extracellular signals

A. Moran[a,*], I. Bar-Gad[a,b]

[a] Gonda Multidisciplinary Brain Research Center, Bar Ilan University, Ramat Gan, Israel
[b] Goodman Faculty of Life Sciences, Bar Ilan University, Ramat Gan, Israel

ARTICLE INFO

Article history:
Received 20 June 2009
Received in revised form 25 October 2009
Accepted 30 October 2009

Keywords:
Extracellular recording
Background unit activity (BUA)
Oscillations
Local field potential (LFP)
Coherence
Spike trains

ABSTRACT

The spatial organization of neuronal elements and their connectivity make up the substrate underlying the information processing carried out in the networks they form. Conventionally, anatomical findings make the initial structure which later combines with superimposed neurophysiological information to create a functional organization map. The most common neurophysiological measure is the single neuron spike train extracted from an extracellular recording. This single neuron firing pattern provides valuable clues on information processing in a given brain area; however, it only gives a sparse and focal view of this process. Even with the increase in number of simultaneously recorded neurons, inference on their large-scale functional organization remains problematic. We propose a method of utilizing additional information derived from the same extracellular recording to generate a more comprehensive picture of neuronal functional organization. This analysis is based on the relationship between the oscillatory activity of single neurons and their neighboring neuronal populations. Two signals that reflect the multiple scales of neuronal populations are used to complement the single neuron spike train: (1) the high-frequency background unit activity representing the spiking activity of small localized subpopulations and (2) the low-frequency local field potential that represents the synaptic input to a larger global population. The three coherences calculated between pairs of these three signals arising from a single source of extracellular recording are then used to infer mosaic representations of the functional neuronal organization. We demonstrate this methodology on experimental data and on simulated leaky integrate-and-fire neurons.

© 2009 Elsevier B.V. All rights reserved.

1. Introduction

The anatomical organization of neuronal elements in the brain, as well as their spatial relationships can provide important clues as to the computational properties of underlying neuronal networks. This spatial organization places constraints on physiological and computational studies targeting the unique features of a neuronal network. By contrast, functional connectivity relates to the correlation between the physiological activities of different neurons (Gerstein and Perkel, 1969; Aertsen et al., 1989; Friston, 1994). Although the term is not well defined across different methodologies such as imaging or extracellular recordings, or even within these methodologies (Horwitz, 2003) it usually refers to the co-activation of several neuronal elements which informs on their connectivity, organization and function. Combining spatial organization and functional connectivity enables the formulation of the functional organization term. For our purposes, functional organization is defined here as the spatial organization of coherent neuronal elements, and does not refer to a specific behavioral function.

Functional organization has been studied over the years using two extreme methodologies: a macroscopic approach that examines large neuronal populations, and a microscopic approach that deals with single neurons. At the macroscopic level, electroencephalography (EEG), positron emission tomography (PET) and functional magnetic resonance imaging (fMRI) have been used to study inter-region functional organization, both at rest and during task related activities (Barlow and Brazier, 1954; Adey et al., 1961; Gevins et al., 1985; Friston et al., 1993; Biswal et al., 1995; Buchel and Friston, 1997; Pfurtscheller and Andrew, 1999). These macroscopic methodologies have low spatial resolution which prevents them from inspecting local features of the functional organization in a certain region or nuclei. On the other hand, the microscopic approach is based on single neuron activity. The neuronal activity is typically derived from extracellular recordings obtained by using microelectrodes. This approach provides high spatial resolution, but probes an extremely sparse sample of the neuronal population even when using mod-

* Corresponding author. Tel.: +972 3 5317141; fax: +972 3 5352184.
E-mail address: anan.moran@live.biu.ac.il (A. Moran).

0165-0270/$ – see front matter © 2009 Elsevier B.V. All rights reserved.
doi:10.1016/j.jneumeth.2009.10.024

ern multi-electrode equipment (Bartho et al., 2004; Buzsaki, 2004).

However, the extracellular signal contains additional information that may be used to bridge the gap between these two extreme approaches and provide multi-scale functional organization information.

The signal picked up by the electrode in the extracellular medium is a summation of a variety of signals derived from many processes and neural elements. These signals include dipoles generated among others by spiking activity (Rall, 1962), postsynaptic potentials (Mitzdorf, 1985) and fluctuations in the membrane voltage (Pedemonte et al., 1998; Goto and O'Donnell, 2001). Spiking activity is reflected primarily in high-frequency changes in the signal (typically >300 Hz), therefore it can be extracted from the raw recorded extracellular signal by a high-pass filter with a cutoff frequency in this range. This time series, termed multi-unit activity (MUA), is the summation of the action potentials of multiple neurons that are in close proximity to the recording electrode. It is based on the principle that the high-frequency spiking signal decays rapidly over distance (Legatt et al., 1980). The distance over which spiking activity may be distinguished from background activity (the summation of more distant neurons) depends on the size and shape of the neurons and on properties of the recording electrode, but is generally on the order of 100–300 μm (Grover and Buchwald, 1970; Henze et al., 2000). The extracellular spike reflects the intracellular action potential but its shape is dependent on multiple properties of the neuron (such as channel concentration, dendritic tree structure) and the location of the electrode relative to the neuron (Henze et al., 2000; Gold et al., 2006).

The activity of individual neurons may be extracted from the MUA and transformed into multiple point processes, where each of the time series represents a separable single-unit spike train (SU-ST) or a non-separable multi-unit spike train (MU-ST). In other words, whereas the MUA is a time series of the sampled and filtered signal representing the overall activity recorded extracellularly from nearby neurons, the MU-ST is a set of point processes which represent spike times of multiple units. Research on the properties of spike trains such as rate, synchronization and patterns has played a major role in furthering our understanding of neuronal processing (Abeles, 1991). The MUA is made up of spiking activity of large or nearby neurons that can be transformed into spike trains (either SU-ST or MU-ST), and background unit activity (BUA). The BUA represents smaller sub-noise level spikes generated by the surrounding neuronal population. By separating the BUA from the MUA small and local neuronal populations can be studied without the bias of larger dominant spikes (Moran et al., 2008).

The low-frequency (typically <300 Hz) changes in the extracellular signal recorded by the microelectrode are termed the local field potential (LFP). This signal is derived from multiple slower processes and is less attenuated over large distances because of its lower frequency. Thus, it can reflect remote processes in the range of 0.5–3.0 mm away from the microelectrode tip (Mitzdorf, 1987; Juergens et al., 1999). Historically, LFP was assumed to arise from excitatory and inhibitory postsynaptic potentials (Mitzdorf, 1985). The LFP was thought to reflect the summation of the input to the local network, as opposed to the MUA which represents the output of the local network (Freeman, 1975; Legatt et al., 1980). However, other slow processes contributing significantly to the LFP have been identified such as membrane oscillations (Pedemonte et al., 1998; Goto and O'Donnell, 2001) and spike hyperpolarization (Buzsaki, 2002). The relationship between the LFP and the various representations of spiking information is complex. In some cases there is significant mutual information between spiking activity and the LFP recorded on the same electrode (Rasch et al., 2008). Other behavioral events can be reflected in only one of the signals, either in the LFP or in the spiking activity (Buchwald et al., 1965).

Periodic oscillations play a cardinal role in the normal function of the nervous system (for a review see Engel et al., 2001; Hutchison et al., 2004; Buzsaki and Draguhn, 2004). Early studies suggested that the oscillatory electroencephalogram (EEG) reflected behavioral states of the brain (Adrian and Matthews, 1934; Brazier, 1949). More recently, oscillations have been identified in different brain areas in the LFP (Bragin et al., 1995; Murthy and Fetz, 1996; Brown and Williams, 2005), MUA (Gray and Singer, 1989; Eeckman and Freeman, 1990), and spike trains (Baker et al., 2003; de Solages et al., 2008). In addition to their normal expression, pathological oscillations have also been found in several cognitive and motor disorders such as epilepsy (Bragin et al., 2002), essential tremor (Halliday et al., 2000; Deuschl and Bergman, 2002), and Parkinson's disease (PD) (Lenz et al., 1988; Bergman et al., 1994; Levy et al., 2002; Brown, 2003).

In this manuscript we present a data analysis method which utilizes the differential manifestation of oscillations in different extracellular signals. This method may be used to shed light on the functional organization of multiple scales of the environment surrounding the microelectrode. A specific implementation of a subset of this analysis method has recently been used by us to characterize the local functional organization of the subthalamic nucleus in Parkinson's disease patients (Moran et al., 2008). The methodology presented below describes the general framework and demonstrates its use on both simulated and experimental data. This broad approach enables the deployment of the techniques on diverse neurophysiological signals recorded in different brain structures during diverse experimental paradigms.

2. Methods

2.1. Animal recordings

The neuronal recordings are from a Cynomologus monkey (*Macaca fascicularis*, male, 4 kg), that underwent 1-methyl-4-phenyl-1,2,3,6-tetrahydropyridine (MPTP) injections leading to a Parkinsonian state. All procedures were in accordance with the National Institutes of Health Guide for the Care and Use of Laboratory Animals and Bar Ilan University Guidelines for the Use and Care of Laboratory Animals in Research and were approved and supervised by the Institutional Animal Care and Use Committee (IACUC). Full details of the experimental protocol appear elsewhere (Erez et al., 2009). Briefly, data were acquired via multiple microelectrodes extended to different nuclei of the basal ganglia through a recording chamber. Extracellular recording was performed via glass-coated tungsten microelectrodes (impedance, 0.25–0.7 MΩ at 1 kHz). The electrode signal was amplified with a gain of 1000 and band-pass filtered with a 2–8000 Hz four-pole Butterworth filter (MCP+ 4.10, Alpha–Omega Engineering, Nazareth, Israel). The signal was continuously sampled at 40 kHz with 14-bit resolution (Alphamap 10.10, Alpha–Omega Engineering) yielding a ~0.5 μV recording amplitude resolution. The continuous digitized signal was later sorted offline (OFS-2.8.4, Plexon, Dallas, TX) to produce SU-STs.

2.2. Simulations

Following earlier work by Zeitler et al. (2006), we constructed a simulated leaky integrate-and-fire (LIF) neuronal environment with partially correlated input. The environment was expanded to control the phase of the correlated oscillatory common drive. Three main components were defined for the single neuron model: (1) The LFP, which forms the total input to the neuron (Fig. 1A,

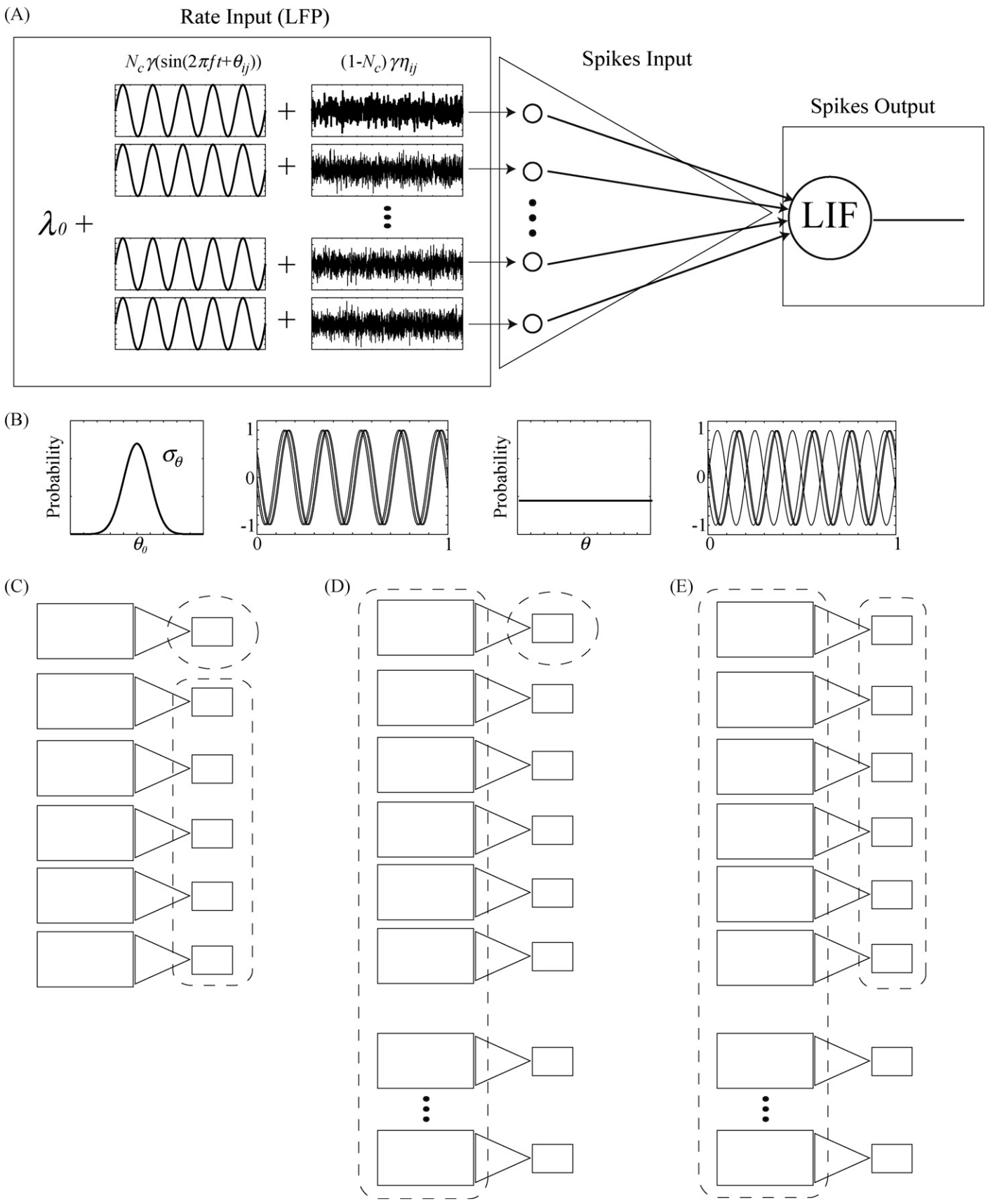

Fig. 1. Simulation framework configuration. (A) Schematic diagram of the input–output configuration of a single leaky integrate-and-fire (LIF) neuron. The rate of the input layer to the neuron (square) is the sum of an oscillatory signal and white noise; this is transformed to point processes of the spiking inputs (triangle) which are fed to the LIF neuron (circle). (B) The distribution of phases is shown using a phase histogram and examples of the resulting oscillatory signals. The phases are chosen from either a narrow Gaussian (left) or a uniform distribution (right). (C–E) Schematic diagrams of the configurations used for testing the relations between different extracellular signals, C: SU-ST vs. BUA, D: SU-ST vs. LFP, E: BUA vs. LFP. *Note*: The local population is defined as excluding the single neuron, thus representing the BUA and not the MUA.

left rectangle). (2) Poisson conversion neurons that transform the input rate into spiking activity (Fig. 1A, middle triangle). A Poisson neuron fires stochastically and its probability of generating a spike at a certain time depends solely on its underlying rate function. (3) LIF neurons receiving input from the conversion neurons (Fig. 1A, right circle). Each of these LIF neurons received 100 spike trains created by the Poisson neurons as input and produced an output spike train using a conductance-based differential equation. To create a simulated neuronal environment with partially correlated and oscillatory LFP, inputs fed to Poisson conversion neurons were comprised of a mixture of individual random white noise $(1-N_c)\gamma\eta_{ij}$ and a sine wave with a random phase $N_c\sin(2\pi ft+\theta_{ij})$. The white noise η_{ij} ($\mu=0, \sigma=1$) was scaled by the common γ factor. Two parameters controlled the degree of correlation between the input drives. The first was the correlation fraction N_c ($0 \le N_c \le 1$) which defines the ratio between the oscillatory and random noise assigned to each of the neurons. Higher values led to higher correlations. The second parameter was the distribution from which the phases of the sine waves were drawn. This was either a narrow Gaussian distribution ($\sigma=0.03$) which simulated a general in-phase relation between different input sources (Fig. 1B, left two panels), or a uniform phase distribution which corresponded to out-of-phase oscillatory input received by different neurons (Fig. 1B, right two panels). A rate constant $\lambda_0=20$ spikes/s was added as a baseline firing rate. The rate input to a conversion neuron j connected to a LIF neuron i was therefore:

$$x_{ij} = \lambda_0 + N_c\gamma\sin(2\pi ft+\theta_{ij}) + (1-N_c)\gamma\eta_{ij} \quad (1)$$

with $\gamma=10$. The LFP surrounding a given LIF neuron i was calculated as the sum of n rate input functions ($n=100$):

$$\mathrm{LFP}_i = \sum_{j=1}^{n} x_{ij} \quad (2)$$

The rate input x_{ij} was converted into spike train y_{ij} by the Poisson neurons (Fig. 1A, small circles in triangle). Each set of n individual spike trains was later fed to a single LIF neuron. The change in membrane potential is given by

$$C\frac{dV}{dt} = -I_e - I_l \quad (3)$$

with membrane capacitance C, excitatory current I_e, leak current I_l, and V as the membrane potential. The currents I_e and I_l are calculated by

$$I_e(t) = G_e(t)\cdot(V(t)-E_e), \qquad I_l(t) = G_l\cdot(V(t)-E_r) \quad (4)$$

where $G_e(t)$ is the instantaneous excitatory conductivity, E_e is the excitatory reversal potential and E_r is the membrane rest potential. The connection between the input spike trains and the membrane conductance is given by

$$G_e(t) = \sum_{i=1}^{n}\sum_{j=1}^{j_i^{\max}} g_e(t-t_i^j) \quad (5)$$

with t_i^j the spike time of the jth spike of neuron i, and g_e an alpha function describing the decay of spike influence over time on membrane conductivity:

$$g_e(t) = \left(g_0\left(\frac{t}{\tau}\right)e^{-(t/\tau)}\right)\cdot\Theta(t) \quad (6)$$

where τ describes the rate of decay, g_0 is the scaling factor and $\Theta(t)$ is the Heaviside function. Values for the above variables followed (Stroeve and Gielen, 2001): $\tau=1.5$ ms, $C=325$ pF, $E_e=0$ mV, $E_r=-75$ mV, $G_l=25$ nS and $g_0=3.24$ nS. At the single neuron level the simulation started with the neuron membrane potential in the rest potential. For each step the next membrane potential was calculated using Eqs. (1)–(6). When the membrane potential reached $V_{thr}=-55$ mV a spike was generated, its time was recorded, and the

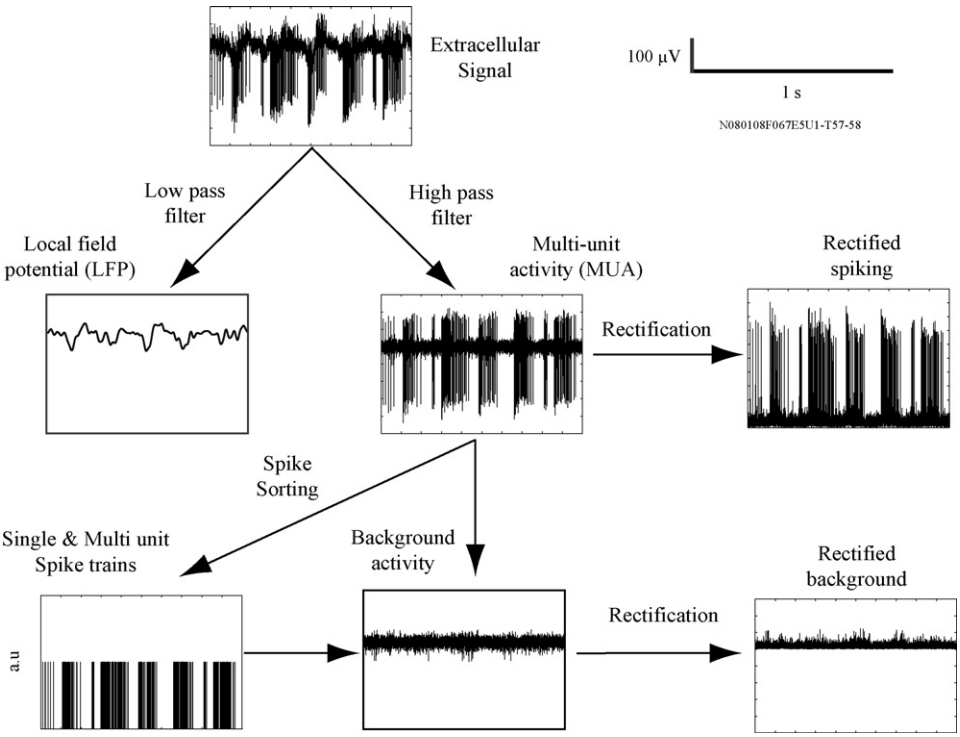

Fig. 2. Diverse signals derived from a single extracellular recording. Box and arrow diagram defining the processing stages (arrows) and derived signals (boxes) from an illustrative extracellular signal recorded in the GPe of a parkinsonian primate. The single and multi-unit spike trains (SU-ST and MU-ST, respectively) are point processes while the rest of the signals are time series representing the continuous sampled signals.

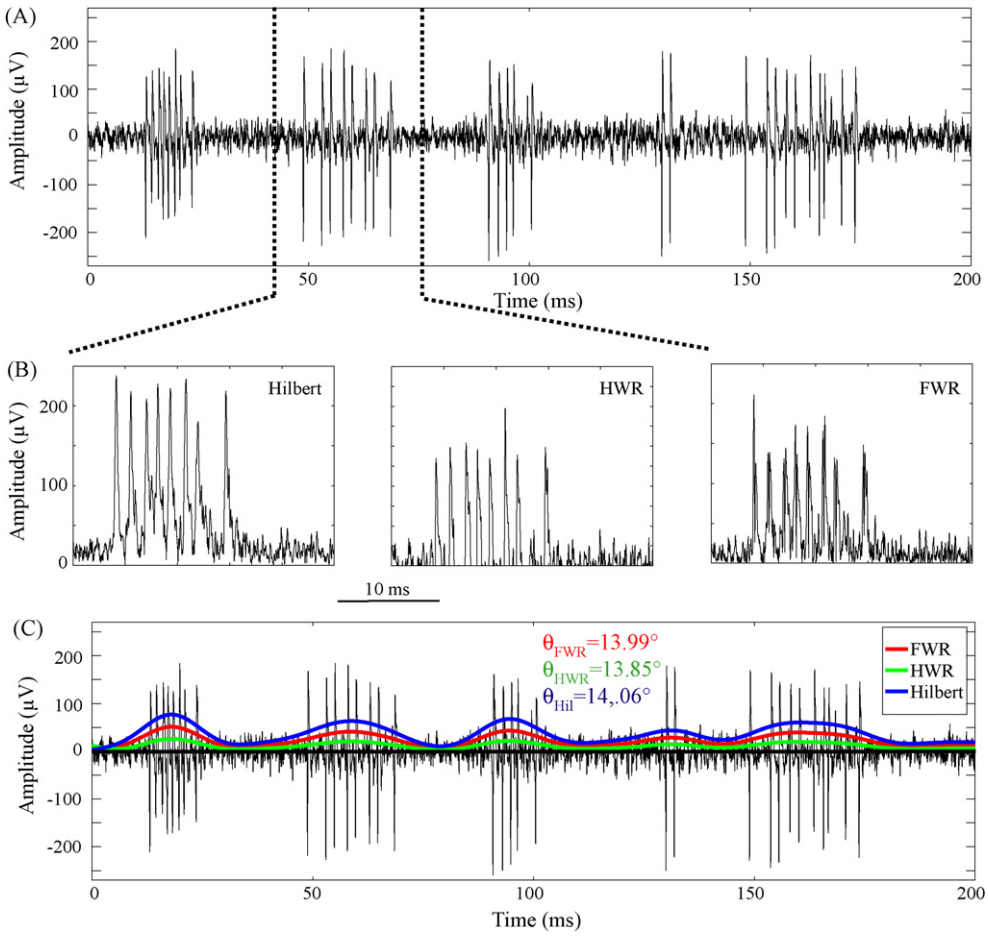

Fig. 3. Envelope construction procedure. (A) Sample high-pass filtered signal. (B) Enlarged rectifying transformations (left to right): Hilbert transform, half wave rectification (HWR), and full wave rectification (FWR). (C) The transformed signals following low-pass filtering (40 Hz, four-pole Butterworth) overlaid on the original signal. The phase of each of the transformation relative to the spike train is shown (θ_{FWR}, θ_{HWR}, θ_{Hil} in the corresponding colors). (For interpretation of the references to color in this figure legend, the reader is referred to the web version of the article.)

membrane potential was reset to E_r. No explicit refractory period was imposed.

Multi-unit activity generation was started by summing the activity of 19 single LIF neurons as previously defined. This could also be presented as the sum of all Dirac delta functions describing the MU-ST:

$$\text{MU-ST}(t) = \sum_{i=1}^{19}\sum_{j}\delta(t - t_i^j) \tag{7}$$

where t_i^j is the jth spike time of ith neuron, and δ is the delta function. Regenerating the MUA employed a process in which each spike timestamp from the MU-ST was replaced by a representative spike shape (taken from the aforementioned experimental data). To carry out this replacement, the spike train was convolved with a spike shape (length 1 ms, 20 sampling points). In the next step, white noise ($\mu = 0$, $\sigma = 30$) was added to the signal and then band-pass filtered using a four-pole Chebyshev Type II filter with cutoff frequencies of 250 and 6000 Hz. Finally the signal envelope was calculated using the Hilbert transform.

2.3. Coherence

Coherence was calculated by normalizing the cross-spectrum between two signals by the multiplication of the square root of their auto-spectrums:

$$C_{xy}(f) = \frac{|P_{xy}(f)|^2}{|P_{xx}(f)| \cdot |P_{yy}(f)|} \tag{8}$$

The magnitude of the coherence is bounded between 0 and 1, reflecting a no to perfect linear correlation between the signals with relation to frequency f, respectively.

The significant coherence limit was calculated by (Rosenberg et al., 1989):

$$C_{\text{limit}} = 1 - (1 - \alpha)^{1/(L-1)} \tag{9}$$

with the level of significance set at $\alpha = 0.999$ and $L = 30$ (number of two second consecutive windows in a 1 min signal).

Coherence was measured between all the pairs formed by the three signals which are illustrated in Fig. 1: SU-ST ↔ BUA (Fig. 1C), SU-ST ↔ LFP (Fig. 1D) and BUA ↔ LFP (Fig. 1E) with different degrees of correlation (N_c) and phase distribution of the common correlated oscillatory drive (σ_θ).

2.4. Software

The MATLAB (V2007B, Mathworks, Natick, MA) software used for the analysis and simulations in this article can be found at: http://neurint.ls.biu.ac.il/software/Osc.

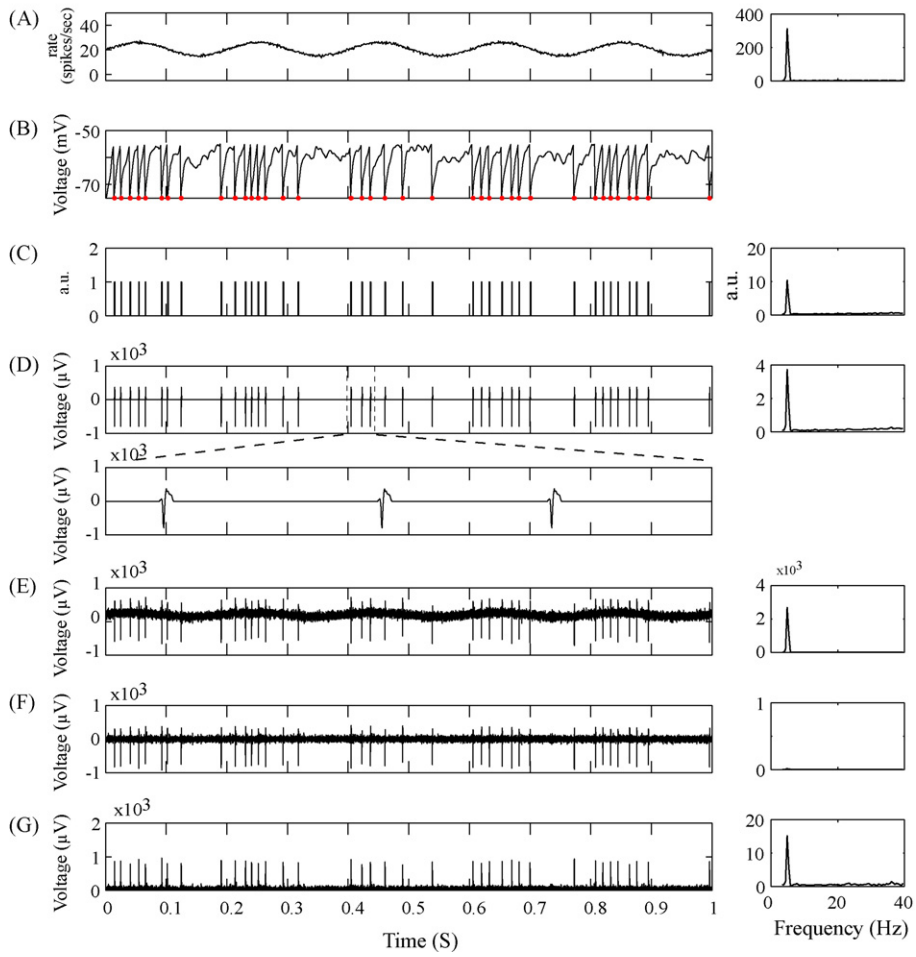

Fig. 4. Simulation of neuronal oscillations. Different neuronal signals are shown throughout the transformation process (left), and their associated PSD (right). (A) Summed input representing the LFP displaying a strong 5 Hz peak. (B) LIF neuron output given the signal in (A) as input. Red dots indicate spiking activity where the LIF neuron crossed the threshold and was reset. (C) Spike train (SU-ST) of the LIF activity presented in (B). The PSD shows the 5 Hz oscillation. (D) Spike times from the signal in (C) were replaced by non-filtered recorded spike shapes. The sampling rate was increased from 1000 Hz to 20,000 Hz to account for this transition. The 5 Hz peak was still significant. (E) The broadband signal was created from a summation of the spikes from (D) and the LFP signal in (A) multiplied by 10. The 5 Hz peak greatly increased. (F) The signal in (E) after 250–6000 Hz band-pass filtering. The 5 Hz peak disappeared from the PSD. (G) The signal in (E) after full wave rectification (FWR). A 5 Hz peak is clearly visible in the PSD. All PSDs were normalized to the mean power in the 250–350 Hz band ($N_c = 0.4$, $p_{\text{phase}} \sim N(\mu = 0, \sigma = 0.03)$). (For interpretation of the references to color in this figure legend, the reader is referred to the web version of the article.)

3. Results

The extracellular signal recorded by a microelectrode conveys the sum of multiple processes related to neuronal elements. Filtering the extracellular signal separates the original signal into two complementary signals: the LFP and MUA (Fig. 2). The cutoff frequency of the filter is typically in the range of 150–300 Hz (low and high-pass filter, for LFP and MUA respectively), to generate the two signals. In some cases the MUA contains distinguishable spikes belonging to one or more separable single neurons which may be identified and assigned to the specific neurons via online or offline spike sorting. Additionally, spikes arising from multiple units which are not separable through sorting may be grouped. The identified spikes are thus assigned to one or more single-unit spike trains (SU-ST) and multi-unit spike trains (MU-ST). The shapes of the spikes identified as belonging to the spike trains may be removed (see procedure below) from the MUA leaving a "spike-free" BUA signal. The low-frequency envelope of any of these high-frequency signals may then be calculated using the rectified signals (Fig. 2).

The amplitude of signals derived from the high-pass filtering of the extracellular signal such as the MUA and BUA may be modulated by low-frequency oscillations (Fig. 3A). This low-frequency envelope can be calculated using a two-stage process: extraction of the instantaneous power of the signal, followed by its smoothing using a low-pass filter. Multiple methods for extracting the instantaneous power of the signal may be used, such as:

- Full wave rectification (FWR): $y(t) = |x(t)|$.
- Half wave rectification (HWR): $y(t) = \begin{cases} x(t) & x(t) > 0 \\ 0 & x(t) \le 0 \end{cases}$.
- Absolute value of the Hilbert transform: $y(t) = \left| \frac{1}{\pi} \cdot PV \int_{-\infty}^{\infty} \frac{x(\tau)}{\tau - t} d\tau \right|$.

Despite the differences in the derived signal among extraction methods (Fig. 3B), the application of a low-pass filter leads to a highly similar envelope for the extracellular recorded neuronal signals (Fig. 3C). The offset of the extracted phase between the different methods is typically $\ll 1^\circ$. This is due to the usage of a significantly lower frequency cutoff (typically <100 Hz) than that of the extracellular spikes and the stereotypic shape of extracellular action potentials.

To study and validate the decomposition of the raw signal we reversed the procedure and integrated several signals while evaluating the PSD after each composition step. The whole procedure

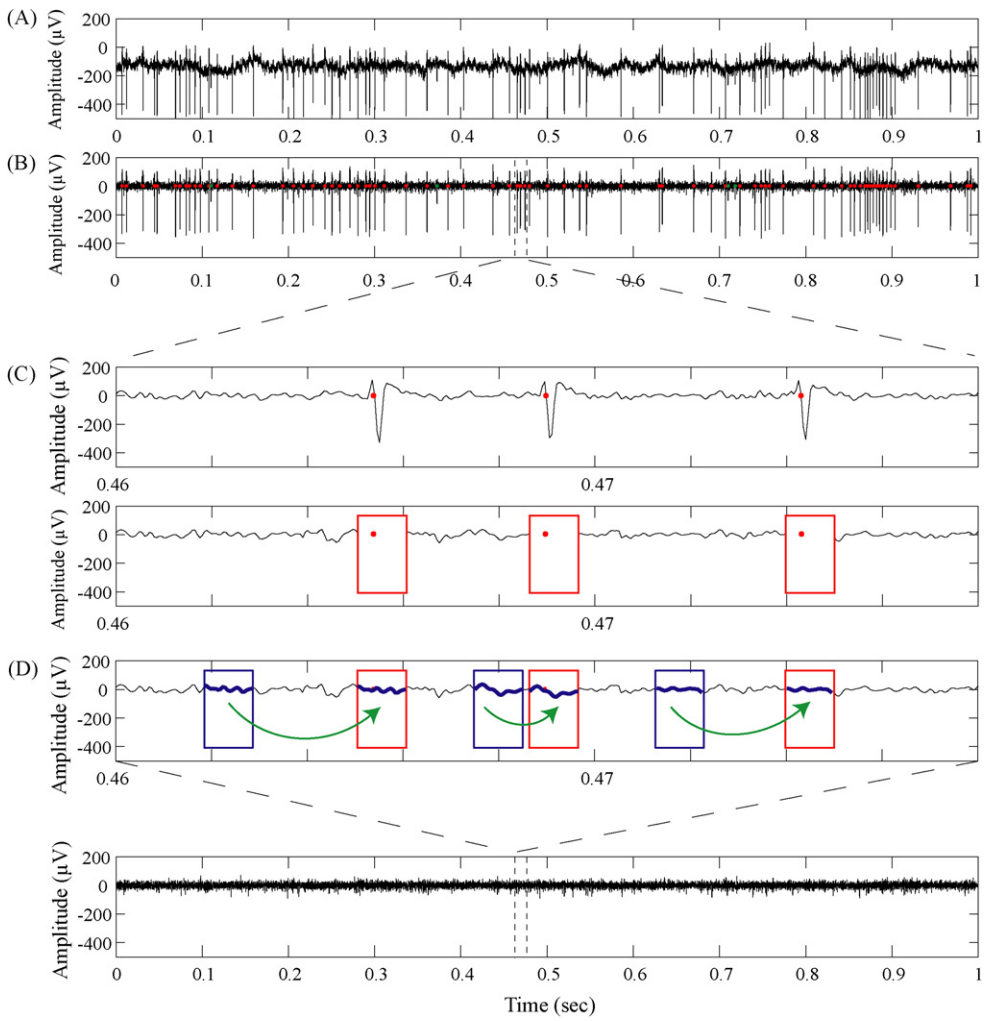

Fig. 5. Background unit activity extraction procedure. (A) Example of a raw signal. (B) The same signal following high-pass filtering (MUA). (C) Identification of spiking activity (red dots) and removal of the surrounding time window (−0.5 to +2.5 around the spike identification point). (D) Replacement of removed spikes by randomly chosen non-spiking windows. The final result of the transformation is the background unit activity (BUA).

is presented using simulated data (Fig. 4). Leaky integrate-and-fire (LIF) neurons each received input from a separate group of 100 Poisson neurons. Each of these Poisson neurons received a mixture of low-frequency (5 Hz) oscillatory input and white noise (see Section 2 for details). The fraction of oscillatory input (N_c) in this example was set to 0.4 and the phases were drawn from a narrow Gaussian distribution. The summed neuronal input (Fig. 4A), following its Poisson conversion to spiking activity, drove the LIF membrane potential (Fig. 4B). The resulting LIF neuron spike train (Fig. 4C) revealed a strong oscillatory component in its power spectral density (PSD). These oscillations were maintained when a spike shape replaced the spike times in the spike train (Fig. 4D) and when the slow input (representing the LFP) was added to the spiking signal to mimic a wide-band recorded signal (Fig. 4E). After high-pass filtering of the wide-band signal, the remaining signal lost its low-frequency components (Fig. 4F). Envelope extraction, however, led to the reappearance of the low-frequency oscillatory component, revealing once again the slow modulations of the burst of spikes (Fig. 4G).

The high-frequency part of the signal recorded by the microelectrode (MUA) contains the single-unit spikes, and multi-unit spikes reflecting a few nearby neurons. In addition it contains a summation of a larger population of more remote or smaller neurons which are classically referred to as generating 'sub-noise level' spikes. Separating the activity of the remote neurons from the larger spikes requires a spike removal procedure (Fig. 5). The preliminary stage is to identify the spike to be removed. Multiple thresholds may be used for detection and can depend on the properties of the neuronal tissue (such as neuronal density and soma size). A general procedure yielding satisfactory results in multiple brain areas is based on a signal to noise (SNR) measure. The neuronal spikes are detected by setting a threshold of 5 standard deviations above and below the mean power of the MUA signal. In the subsequent step the traces in the segments surrounding each of these spike timestamps in the MUA signal are replaced by a spike-free segment from a random location within the same recorded trace leading to the construction of the BUA. The length of the segment and its location relative to each spike may be different and depend on the shape and length of the extracellular spike. These vary drastically between brain areas and cell types. In the vertebrate central nervous system in general, segments starting 0.5 ms prior to the spike timestamp and ending 2.5 ms after that timestamp leave only negligible energy associated with the spike. The small inconsistencies between the original and the inserted spike-free segments do not significantly increase power in the low-frequency band because these inconsistencies are in the range of the sampling rate which is usually very high. With a sufficiently wide spike removal window the boundaries of the inserted signal are in the range of the noise. This reduces their influence on low-frequency power.

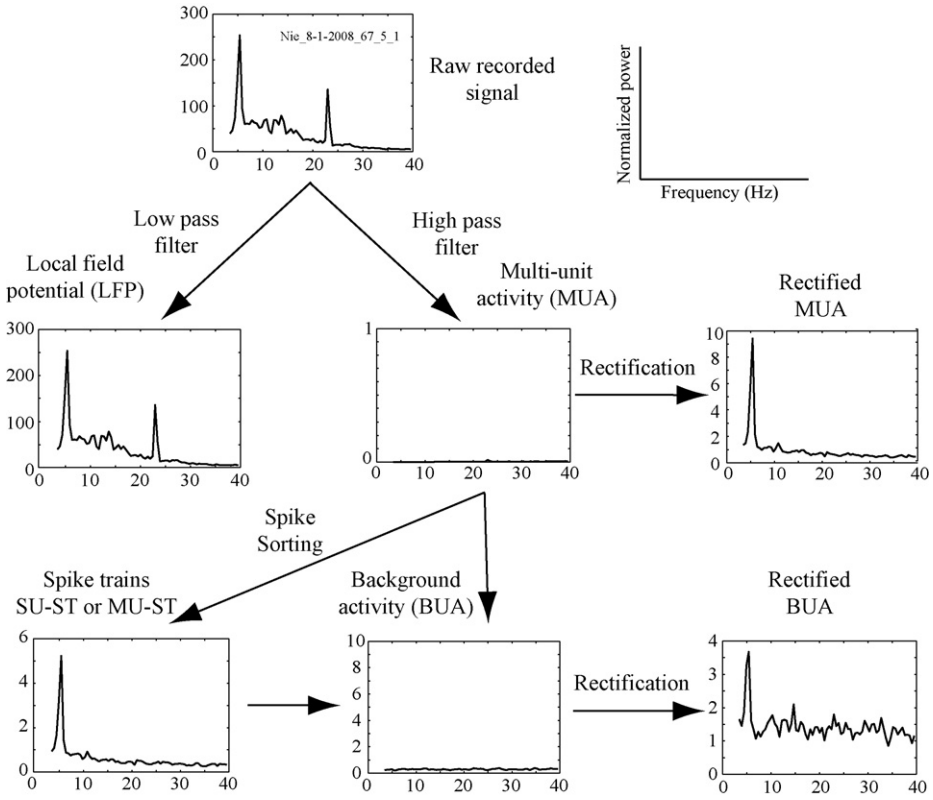

Fig. 6. Low-frequency oscillations in extracellular signals. Power spectral density (PSD) graphs of the signals presented in Fig. 2. The low-frequency oscillations which exist in the LFP do not appear in the MUA or the BUA. The oscillations are apparent again in these signals following the rectification process. All PSDs were normalized to the mean power in the 250–350 Hz band of the signal.

To examine the experimentally recorded data in the lower frequency domain we applied spectral analyses to the raw (wide-band) signal of a globus pallidus external segment (GPe) neuron of a Parkinsonian primate as well as its derived signals (Fig. 2). The raw signal, LFP and spike train were directly spectrally analyzed, while the BUA and MUA were spectrally assessed following envelope extraction (Fig. 6). The power was normalized to represent the power in a certain frequency relative to the mean power in the 250–350 Hz frequency band of that signal. The raw signal presented two sharp peaks near 5 and 22 Hz. These peaks were clearly seen in the LFP signal but were filtered out by the high-pass filtering of the MUA. The PSD of the extracted spike train revealed that this signal only maintained the 5 Hz peak. Removal of these spikes from the MUA led to a BUA which did not display any of the peaks. The rectification process of both the MUA and the BUA revealed the low-frequency modulation of the signal and allowed the 5 Hz peaks to reemerge. The increased power around 22 Hz was limited to the LFP and may be due to non-linear transformations performed by the neurons on the input. The transformation performed by the GPe neurons led to filtering of the high-frequency input whereas the lower frequency oscillations presented in their output were maintained, as is clearly visible in the SU-ST, MUA and BUA (Fig. 6).

The relation between the different signals in the frequency domain was analyzed using a coherence measure that normalizes the squared cross-spectrum of two signals by dividing by both auto-spectrums. An example of this method is presented using an extracellular signal recorded in the subthalamic nucleus (STN) of a non-human primate model of Parkinson's disease (MPTP treated) (Fig. 7). The raw unfiltered signal was used to produce the three derived signals of the LFP, SU-ST and the BUA envelope (Fig. 7A), and each of their low-frequency modulations was extracted (Fig. 7B). The PSD of the three signals showed a distinct peak near 13.5 Hz (Fig. 7C). Coherence analysis was then used to assess the linear relation and phase shift between these signals. In this example, the coherences between all three signals were significant at 13.5 Hz (Fig. 7D). Moreover, phase analysis showed that SU-ST and BUA were oscillating almost in-phase (i.e. with zero time delay between the primary neuron and its surrounding neuronal population), while there was about a 114° phase shift between LFP and the two other signals in this frequency. This shift represents a time-lag of about 25 ms between the LFP and the neuronal output signals. In this respect coherence analysis serves to relate co-oscillations of the different signals and thus sheds light on their tendency toward co-activation.

The study assumes different effective ranges of decay between the LFP and BUA signals. To confirm this difference we have inspected the coherence and correlation between LFP–LFP and BUA–BUA signals pairs recorded extracellularly in the globus pallidus of two monkeys at distances of 1–2 mm (Fig. 8). A total of 104 pairs of concurrently recorded signals from different electrode pairs were processed: LFPs were extracted from the raw signals by using a low-pass filter (5th order Chebyshev II with a cutoff at 100 Hz) and BUAs were constructed as described above. Both low-frequency coherence (with a 1 Hz resolution, and the absolute values of BUAs) and overall correlation between each pair were calculated. The two analyses confirmed the basic difference between the relations of these signals. In the coherence domain LFP pairs showed significantly higher coherence than the BUA pairs along the 2–40 Hz spectrum range (Fig. 8C). Collapsing over all frequencies, the mean correlation of the two groups revealed the same significant difference (paired Student's t-test, $p < 0.001$) (Fig. 8D). These results support the different decay properties of the two signals, with high coherence and correlation of LFP versus low coherence and correlation values for the BUA over millimeter range distances.

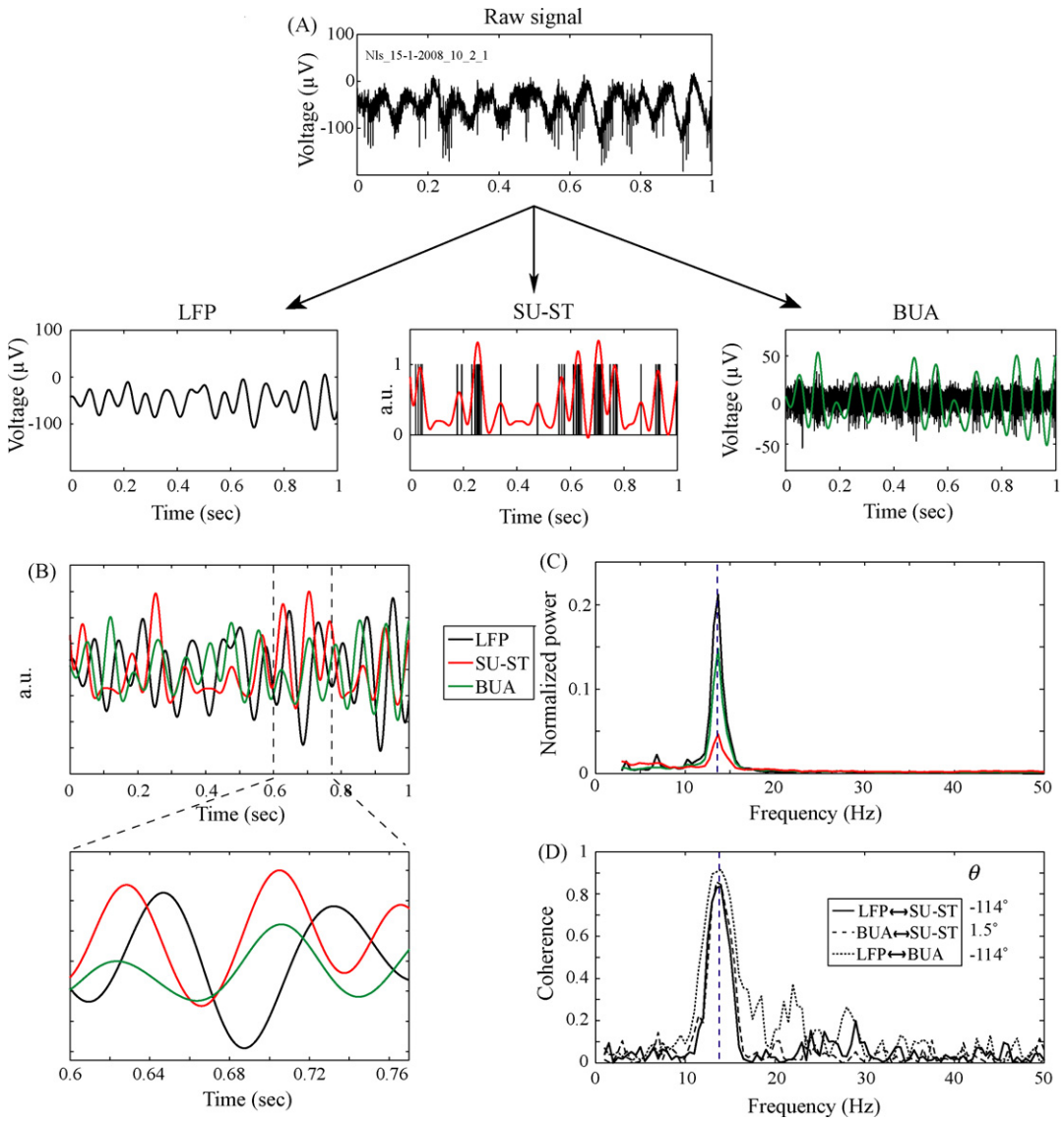

Fig. 7. Coherence between different extracellular signals. (A) The raw, unfiltered, extracellular signal recorded in the STN of a non-human primate model of PD was the source of the three derived signals of the LFP, SU-ST and BUA envelope. The SU-ST and the BUA envelope were then low-pass filtered (cutoff at 20 Hz) to produce their low-frequency modulations (red and green lines, respectively). (B) Superposition of the three low-frequency modulations of the signals (lower panel presents a close-up). (C) Power spectral density of the three derived signals. The peak frequency of all signals is at 13.5 Hz. (D) Coherence of the three derived signals. θ values are the phases between signals in the peak frequency (13.5 Hz) calculated from the cross-spectral density. (For interpretation of the references to color in this figure legend, the reader is referred to the web version of the article.)

Simulations were used to further study the relations of common oscillatory power, connectivity and coherence across the SU-ST, BUA and LFP. We used an environment of 20 LIF neurons (simulating the output neurons or the 'recorded' single units), each of which received spike train input from 100 Poisson neurons which stochastically converted the input LFP into spike trains (Fig. 1A). As LFP is assumed to mainly reflect synaptic activity, it can be modeled as the sum of the rate functions which drive the presynaptic neurons. This input LFP was set to the sum of two components: sine waves and a white noise. The level of input oscillation was controlled by the scalar parameter N_c which set the fraction of oscillatory versus white noise in the input. Another parameter which controlled the strength of correlation was the phase distribution function from which the phase of the oscillatory drive was drawn. In our study it was either uniformly distributed, reflecting a non-correlated out-of-phase oscillatory drive, or a narrow Gaussian distribution reflecting a high similarity in the oscillation drive (Fig. 1B). To study the influence of the level of input oscillatory drive (N_c) on the coherence across the three signals separately from the phase distribution parameter, we used phases from a narrow Gaussian ($\sigma = 0.03$) and changed the N_c parameter from a very low oscillatory fraction (0.005) to a highly correlated input (0.4). Decreasing N_c led to reduced oscillation in the BUA (Fig. 9A), which was evident both visually on the BUA trace and using spectral analysis methods. Coherence of the BUA with SU-ST decreased with N_c reduction but was below statistical significance only when N_c was below 0.05 (Fig. 9B). Varying levels of oscillatory drive (N_c) drastically altered the oscillations in the LFP (Fig. 9C). This produced similar coherence results with SU-ST but typically higher values than those for coherence with the BUA (Fig. 9D).

Several biologically plausible functional organizations were simulated and the paired coherences between all three signals were assessed to examine whether the functional organization could be inferred from the results (Fig. 10). The configurations were built on the framework presented in detail in Section 2 (Fig. 1). The first scenario was a single oscillatory neuron which was a member of a

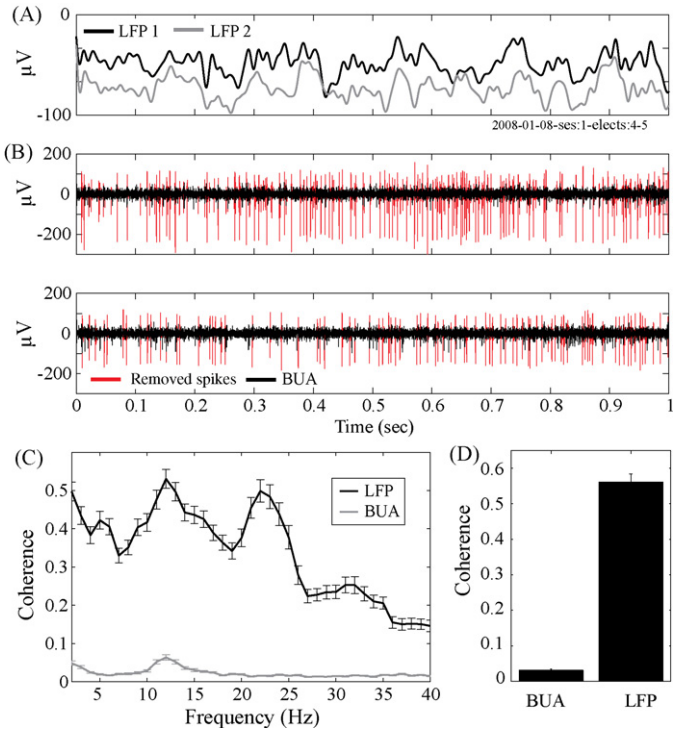

Fig. 8. Different effective range between LFP and BUA. (A) One second long traces of two concurrently recorded LFP signals from electrodes spaced ~1 mm apart. LFPs were extracted from the raw signals using low-pass filter (5th order Chebyshev II, 100 Hz cutoff). (B) The same raw signals as in (A) were used to extract the high-passed signals and consequently to reconstruct the BUAs (BUA—black, removed spikes—red). (C) Coherence between of LFP pairs and rectified BUA pairs ($n = 104$). (D) Correlation between pairs of LFPs and pairs of rectified BUAs signals. Error bars in (C) and (D) represent SEM. (For interpretation of the references to color in this figure legend, the reader is referred to the web version of the article.)

highly oscillatory ($N_c = 0.4$), closely phased local oscillatory neural population surrounded by a large volume of Poisson firing non-oscillatory neurons (Fig. 10A). In this scenario significant coherence was only found between the SU-ST and BUA. The second scenario was a highly oscillatory ($N_c = 0.4$) and closely phased global neuronal population (Fig. 10B). In this scenario significant coherence was found between all three paired coherences. The third scenario presented a low oscillatory ($N_c = 0.005$) closely phased local and global oscillatory population (Fig. 10C). Here, significant coherence was only found in the BUA–LFP relation. The fourth scenario explored another scenario of a highly oscillatory ($N_c = 0.4$), yet out-of-phase, local and global oscillatory populations (Fig. 10D). In this situation significant coherence was found only between SU-ST and the LFP.

4. Discussion

This study presents a novel methodology to infer the functional organization of neuronal tissue on the basis of the coherence between slow oscillatory activities in different extracellular signals. Three signals were derived from the raw recorded extracellular signal and their oscillatory activity was assessed. (1) Single neuron oscillations were quantified based on the spike train identified by spike sorting of the high-pass filtered recording. (2) Large population oscillations were quantified based on LFP oscillations identified using the low-pass filtered recorded signal. (3) Small population oscillations were defined using the background unit activity derived from the rectified, spike-removed high-pass filtered recording. The relations between the oscillations of these signals as depicted by their coherence imply different functional architectures in the surrounding neuronal population. We applied these methods to the oscillating signals in the basal ganglia of a Parkinsonian primate and demonstrated that these oscillations may be replicated by a simulated environment of LIF neurons. The simulation setup allowed us to investigate the relations between different functional organizations and the resulting coherence between signals.

Modern studies of neural information encoding have focused on the point processes representing spike trains of well isolated single units (Abeles, 1991). Historically, analysis of multi-unit activity (MUA) was widespread (Freeman, 1975) but is now mainly restricted to studies in which electrodes (typically macro or lower impedance electrodes) are used and where separation into single units is impossible (but see Schwartz, 2004; Hasenstaub et al., 2007 for modern uses of MUA). The study of MUA using microelectrodes has been further limited by the distortion created by dominant large neurons and has thus been confined to cases in which no large single units are identified on the electrode. Our study presents a methodology for removing the dominant spikes, and produces a signal which is the sum of a larger population of neurons located more distally from the electrode, the BUA. Unlike MUA, the BUA signal provides a unique opportunity to relate the summed activity of a localized network to the activity of one or more single neurons (SU-STs) within the same area. The critical importance of the properties of this relation was underscored in our recent article (Moran et al., 2008) where we showed that although dominant neurons may oscillate, thus causing oscillatory MUA, their BUA did not display significant oscillations, and hence pointed pointing to a out-of-phase oscillatory population or a non-oscillatory population.

The amplitude of the action potential decays exponentially with the distance from the neuron and its decay constant depends on the radius of the soma (Rall, 1962). Thus, the distance from the recording electrode and soma size are the major components determining the extracellular action potential size (although see Lemon, 1984; Henze et al., 2000; Gold et al., 2006 for other components such as the neuron shape and electrode position relative to the dendritic tree). In most areas of the CNS where the size of the soma varies between 10 and 40 μm, neurons at a distance of less than roughly 150 μm may be identified as single units over a noise level of approximately 50–100 μV (Henze et al., 2000); for a discussion on the expected density of neurons versus the actual neurophysiologically identifiable neurons (see Robinson, 1968). Units within a diameter of roughly 200–300 μm around the electrode form most of the multi-unit signal, depending on the soma size and packing of the surrounding tissue (Lemon, 1984; Logothetis, 2002). The number of neurons within this diameter varies greatly depending on the brain structure and the electrode parameters used but is roughly on the order of 10^2 (Robinson, 1968). Identification of oscillatory activity in the summed activity of multiple neurons (such as in the BUA) is significantly easier than for the activity of single neurons and may extend beyond these radii (Huang and Buchwald, 1977; Arezzo et al., 1979). Thus, even in the presence of separable single units in the recorded signal, the background activity may provide a more robust signal for identifying and estimating low-frequency oscillation. Throughout this study we used only the BUA instead of the raw MUA, which contains the large single-unit spikes. This is because relating the spike train to the envelope of the MUA would lead to an inevitable common effect of the spikes on both signals which would bias the phase of their relation toward zero. By contrast, the low-frequency changes in the raw extracellular recorded signal (i.e. LFP) primarily represent slow processes in the neuronal tissue such as synaptic activity, membrane potential oscillations and spike hyperpolarizations (Logothetis, 2003). Slow modulation of spiking activity may also contribute to the LFP, but this contribution was found to be negligible with respect to the other sources

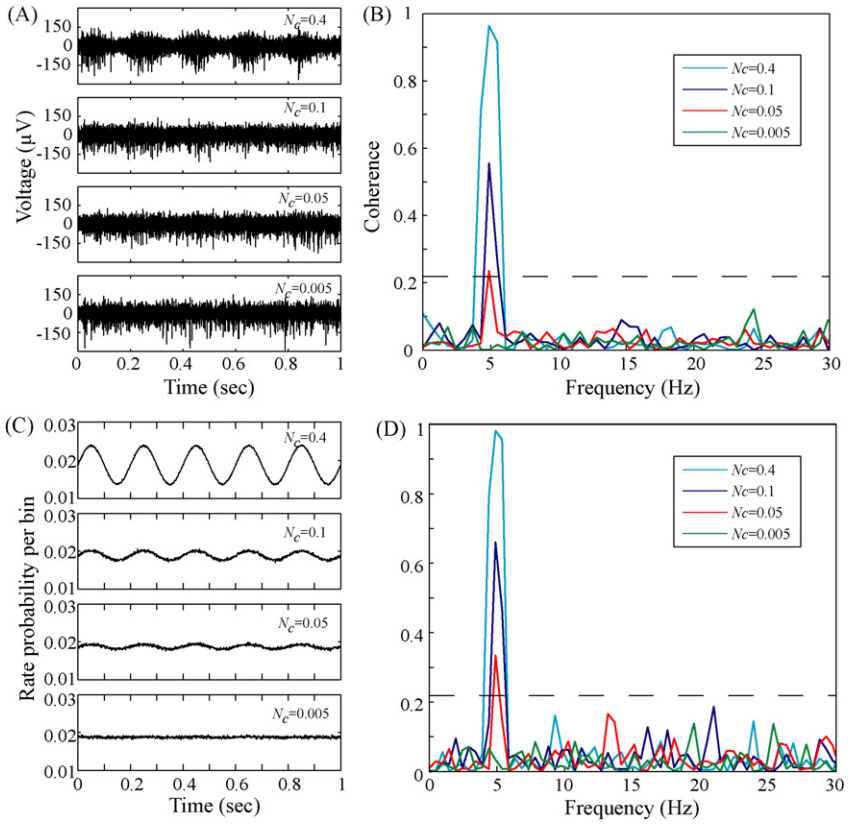

Fig. 9. Coherence between simulated signals. (A) BUA of 19 LIF neurons. Each neuron's spike time was replaced by a spike shape and all spikes were summed and a white noise ($\mu = 0$, $\sigma = 30$) was added. Variable fractions of oscillatory inputs (N_c) were used. (B) Coherence between the spike train of a single LIF neuron created with the same N_c parameter as the other 19 neurons and the constructed BUA presented in (A). (C) The summed input (LFP) to the simulated neurons using the same fractions of oscillatory drives as (A). (D) Coherence between a single LIF neuron created with the same N_c parameter as the LFP presented in (C).

mentioned above (Logothetis, 2002). Low-frequency signals have a slower decay over space leading to detectible oscillations over millimeters or even centimeters in the extreme case of electroencephalography (EEG) or electrocorticography (ECoG). The exact range influencing the LFP in a certain location is dependent on many parameters such as species, brain region and electrode parameters; however, within a certain location the spatial influence is fundamentally different, by orders of magnitude, between LFP and BUA (as a derivative of the MUA) (Mitzdorf, 1987; Juergens et al., 1999; Logothetis, 2002). This difference in spatial influences between the different derived signals is a key parameter which underlies our analysis. Our study supports existing data (Mitzdorf, 1987; Gray et al., 1995; Juergens et al., 1999; Henze et al., 2000; Logothetis, 2003; Goense and Logothetis, 2008) demonstrating that over a millimeter range distances, the decay of the low-frequency LFP is small yielding a highly correlated signal (~0.5) while the high-frequency nature of the BUA leads a large decay yielding only minor correlations (~0.01) resulting probably from active processes. The data does not prove directly the source or decay parameter but provides additional support to the existing vast body of evidence underlying our understanding of the two signals. Further multi-scale studies providing evidence regarding micro- and macroscale activity such as the combination of imaging and electrophysiology may improve our understanding of the exact nature of the different signals.

Neuronal oscillations play a crucial role in the neurophysiology of the CNS. Oscillatory activity in which a single neuron fires spikes with a specific phase relation to a small band of frequencies may be reflected in coherent activity with other neurons in the localized or generalized population. Thus, oscillatory activity is readily recorded in different extracellular signals such as SU-ST, MUA and LFP (Engel et al., 2001; Hutchison et al., 2004; Buzsaki and Draguhn, 2004). The functional organization of neurons within neuronal tissue determines the signals which display the oscillatory activity. Single neuron (SU-ST) oscillations are apparent when the oscillation frequency maintains a non-random distribution. A local population of neurons (MUA or BUA) will display oscillatory activity only when its activity involves the same frequencies with at least a partially in-phase phase distribution. The global input to the population of neurons (LFP) maintains significant oscillatory power based on the total phase distribution. Measuring the coherence between these three oscillatory activities enabled us to infer the different functional organizations of the neuronal tissue.

We tested four common organizations of neural populations using our simulation framework (Figs. 1 and 10). The first configuration reflects synchrony in a small population of neighboring neurons positioned within a global population of non-oscillatory neurons (or out-of-phase neurons). In this configuration the coherence between the spiking train of the SU-ST and BUA yielded high values. When the neuronal population was localized, its contribution to the overall population was small, resulting in negligible coherence of both the SU-ST and the BUA with the LFP. In addition, because the LFP primarily represents the input to the neurons, a lack of coherence may be due to locally generated oscillations which are not part of the input signal to the network. The second configuration mimicked coherent activity within a larger and homogenous population, resulting in significant coherence between all the signals. A coherent activity spanning a large but sparse population results in significant coherence between the LFP and the background but

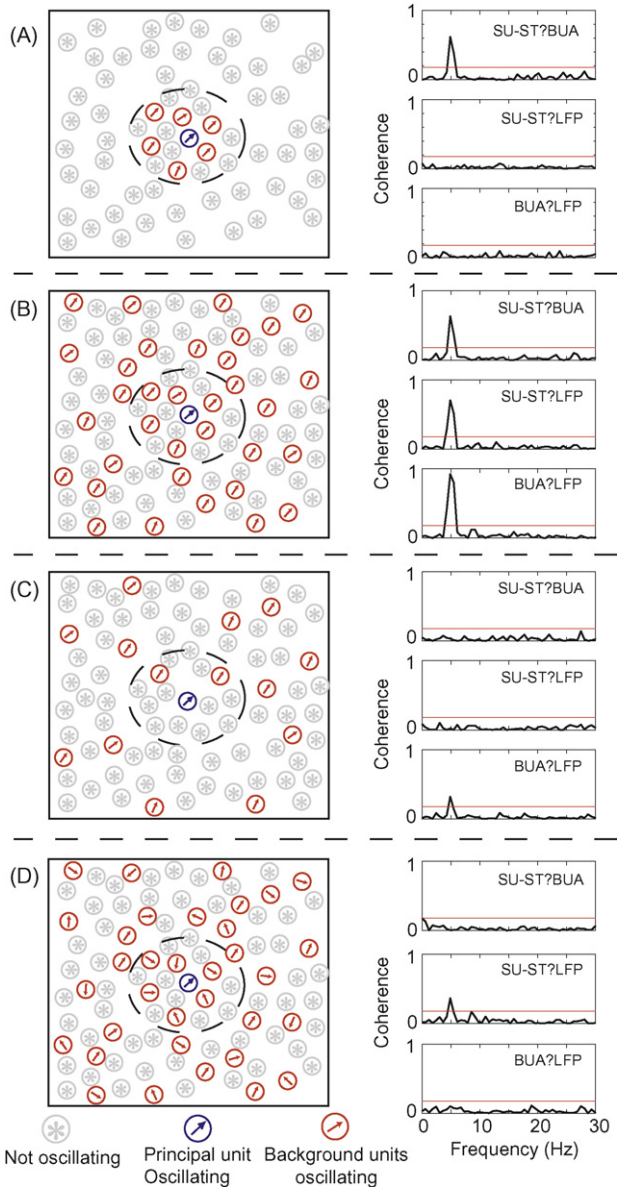

Fig. 10. Relating coherence of neural oscillations to functional organization. Four neuronal functional organization scenarios (left), and the derived coherences between SU-ST, BUA envelope and LFP (right). The arrow circled in blue represents the oscillatory SU-ST picked up by the recording electrode. Arrows circled in red represent other oscillating neurons at the same frequency. The dashed line delimits the area where BUA activity can be detected by the recording electrode. The red line in the coherence graphs marks the $p < 0.001$ significance limit. (A) Isolated highly correlated ($N_c = 0.4$) and closely phased local population of oscillatory neurons in a global non-oscillatory population. (B) Highly correlated ($N_c = 0.4$) and closely phased local and global oscillatory population. (C) Sparsely correlated ($N_c = 0.005$) and closely phased local and global oscillatory population. (D) Highly correlated ($N_c = 0.4$), but uniformly phase distributed local and global oscillatory population. (For interpretation of the references to color in this figure legend, the reader is referred to the web version of the article.)

negligible coherence with the spike trains of individual neurons (Zeitler et al., 2006). Finally, oscillatory activity within a large population which varies in its phases across the neurons resulted in low coherence that was dependent on the phase distribution of the surrounding neurons. This was due to the finite number of oscillators which does not sum to zero, as expected from an infinite sum of sinusoidal waves. It is important to note that we do not claim to have any information about the synaptic connectivity between neurons, but rather only their spatial organization. This is crucial when drawing conclusions from the data. For example, when observing the LFP, this method will not enable the identification of the source of the driving synaptic input, whether outside the specific tissue or caused by collaterals within the same neural tissue. Rather, the analysis can characterize the functional organization of the synaptic input as previously defined.

The simulated data used as a test case for the implementation of the analysis methods were constructed with an input set of pure sine waves. This enabled us to control for the oscillation frequency and phase of the oscillatory input, so that simple analytical and computational analyses could be applied. This, however, is clearly not the case for experimentally recorded neuronal signals. Biological oscillations generally tend to exhibit frequency drifts, even when they have a general tendency to display a characteristic frequency. Apart from the frequency, the phase of the oscillation also shifts, or is influenced by a non-periodic change which cause phase shifts (Hurtado et al., 2004, 2005). Coherence analysis is very sensitive to frequency and phase drifts which cause its values to drop below significance levels. This is also why it is harder to see significant coherence between SU-ST and LFP whereas it is easier to detect them in the MUA–LFP relation where the drifts are summed together and show stronger correlated activity. The simplified oscillation model used in this study enables the definition of qualitatively different organizations of neuronal environments. Expansion of the computational study to include more biologically plausible oscillatory characteristics is important for predicting the magnitude of the expected coherence and providing a numerical or quantitative assessment of the populations of co-oscillating neurons in neighboring and remote areas.

Bridging the gap between the organization (anatomy) of the brain and its function (physiology) has been a challenge since the early studies of the nervous system. Anatomical studies have attempted to tackle this issue through tracing studies designed to identify the connectivity needed to perform a specific function. The main advantage of the anatomical approach is that it can explore thousands of neurons, and directly answer the connectivity question. Its main drawbacks, however, are that it must be done in vitro rather than in vivo, and the fact that there is no true functional connectivity assessment (e.g. silent synapses). Other methodologies that have approached this question include single-unit correlations (Bartho et al., 2004), which are limited to describing a tiny sample within the neuronal population, spike triggered averages (Rieke et al., 1997) that attempt to link a single neuron to the LFP representing its input, and microelectrode recording during fMRI (Logothetis, 2002) relating a single cell to more generalized brain activity. We presented a way of utilizing a recording from just one extracellular electrode to infer information about both local and global populations surrounding the recorded neuron.

This manuscript focused on the application of the method to oscillatory activity recorded from one microelectrode to infer the functional organization. Its scope, however, may be expanded to incorporate both non-oscillatory signals and input from multiple electrodes. It can be adapted to the non-oscillating domain by using temporal correlations or external-event triggered responses between the different signals (SU-ST, BUA and LFP). Assessing the relation of both measures in close temporal proximity versus remotely timed interactions makes it possible to estimate the strength of co-activity of the single neurons and their surrounding local and global populations. Extending the framework to multiple simultaneously recorded electrodes (as is common in both static arrays and independently movable electrodes) may lead to the identification of related local populations and their response to partially overlapping global input.

The method presented in this manuscript enables the reconstruction of the basic functional organization of neuronal areas based solely on existing neurophysiological data. Shedding light on the spatial organization of neuronal elements is an important step toward uncovering the computation which may be performed by the neural elements and the localized networks they form. This functional organization of neuronal systems is thus an essential key to understanding the information processing carried out within these structures in states of health and disease.

Acknowledgments

This work was supported in part by ISF grants (1000-05 and 1698-07) and by the Ministry of Health (MOH-3-4033). The authors thank H. Czitron, A. Tzameret, Y. Erez and K. McCairn for their help in data acquisition. We thank Prof. Hagai Bergman and Dr. Zvi Israel for helpful discussions.

References

Abeles M. Corticonics, neural circuits of the cerebral cortex. Cambridge: Cambridge University Press; 1991.
Adey WR, Walter DO, Hendrix CE. Computer techniques in correlation and spectral analyses of cerebral slow waves during discriminative behavior. Exp Neurol 1961;3:501–24.
Adrian ED, Matthews BHC. The berger rhythm: potential changes from the occipital lobes in man. Brain 1934;57:355–85.
Aertsen AM, Gerstein GL, Habib MK, Palm G. Dynamics of neuronal firing correlation: modulation of "effective connectivity". J Neurophysiol 1989;61:900–17.
Arezzo JF, Legatt ADFAU, Vaughan Jr HG. Topography and intracranial sources of somatosensory evoked potentials in the monkey. I. Early components. Electroencephalogr Clin Neurophysiol 1979;46:155–72.
Baker SN, Pinches EM, Lemon RN. Synchronization in monkey motor cortex during a precision grip task. II. Effect of oscillatory activity on corticospinal output. J Neurophysiol 2003;89:1941–53.
Barlow JS, Brazier MA. A note on a correlator for electroencephalographic work. Electroencephalogr Clin Neurophysiol 1954;6:321–5.
Bartho P, Hirase H, Monconduit L, Zugaro M, Harris KD, Buzsaki G. Characterization of neocortical principal cells and interneurons by network interactions and extracellular features. J Neurophysiol 2004;92:600–8.
Bergman H, Wichmann T, Karmon B, DeLong MR. The primate subthalamic nucleus. II. Neuronal activity in the MPTP model of parkinsonism. J Neurophysiol 1994;72:507–20.
Biswal B, Yetkin FZ, Haughton VM, Hyde JS. Functional connectivity in the motor cortex of resting human brain using echo-planar MRI. Magn Reson Med 1995;34:537–41.
Bragin A, Jando G, Nadasdy Z, Hetke J, Wise K, Buzsaki G. Gamma (40–100 Hz) oscillation in the hippocampus of the behaving rat. J Neurosci 1995;15:47–60.
Bragin A, Wilson CL, Staba RJ, Reddick M, Fried I, Engel Jr J. Interictal high-frequency oscillations (80–500 Hz) in the human epileptic brain: entorhinal cortex. Ann Neurol 2002;52:407–15.
Brazier MAB. The electrical fields at the surface of the head during sleep. Electroencephalogr Clin Neurophysiol 1949;1:195–204.
Brown P. Oscillatory nature of human basal ganglia activity: relationship to the pathophysiology of Parkinson's disease. Mov Disord 2003;18:357–63.
Brown P, Williams D. Basal ganglia local field potential activity: character and functional significance in the human. Clin Neurophysiol 2005;116:2510–9.
Buchel C, Friston KJ. Modulation of connectivity in visual pathways by attention: cortical interactions evaluated with structural equation modelling and fMRI. Cereb Cortex 1997;7:768–78.
Buchwald JS, Halas ES, Schramm S. Comparison of multiple-unit and electroencephelogram activity recorded from the same brain sites during behavioural conditioning. Nature 1965;205:1012–4.
Buzsaki G. Theta oscillations in the hippocampus. Neuron 2002;33:325–40.
Buzsaki G. Large-scale recording of neuronal ensembles. Nat Neurosci 2004;7:446–51.
Buzsaki G, Draguhn A. Neuronal oscillations in cortical networks. Science 2004;304:1926–9.
de Solages C, Szapiro G, Brunel N, Hakim V, Isope P, Buisseret P, et al. High-frequency organization and synchrony of activity in the Purkinje cell layer of the cerebellum. Neuron 2008;58:775–88.
Deuschl G, Bergman H. Pathophysiology of nonparkinsonian tremors. Mov Disord 2002;17(Suppl 3):S41–8.
Eeckman FH, Freeman WJ. Correlations between unit firing and EEG in the rat olfactory system. Brain Res 1990;528:238–44.
Engel AK, Fries P, Singer W. Dynamic predictions: oscillations and synchrony in top-down processing. Nat Rev Neurosci 2001;2:704–16.
Erez Y, Czitron H, McCairn K, Belelovsky K, Bar-Gad I. Short-term depression of synaptic transmission during stimulation in the globus pallidus of 1-methyl-4-phenyl-1,2,3,6-tetrahydropyridine-treated primates. J Neurosci 2009;29:7797–802.
Freeman WJ. Mass action in the nervous system. New York: Academic Press; 1975.
Friston KJ. Functional and effective connectivity in neuroimaging: a synthesis. Hum Brain Mapp 1994;2:56–78.
Friston KJ, Frith CD, Liddle PF, Frackowiak RS. Functional connectivity: the principal-component analysis of large (PET) data sets. J Cereb Blood Flow Metab 1993;13:5–14.
Gerstein GL, Perkel DH. Simultaneously recorded trains of action potentials: analysis and functional interpretation. Science 1969;164:828–30.
Gevins AS, Doyle JC, Cutillo BA, Schaffer RE, Tannehill RS, Bressler SL. Neurocognitive pattern analysis of a visuospatial task: rapidly-shifting foci of evoked correlations between electrodes. Psychophysiology 1985;22:32–43.
Goense JB, Logothetis NK. Neurophysiology of the BOLD fMRI signal in awake monkeys. Curr Biol 2008;18:631–40.
Gold C, Henze DA, Koch C, Buzsaki G. On the origin of the extracellular action potential waveform: a modeling study. J Neurophysiol 2006;95:3113–28.
Goto Y, O'Donnell P. Network synchrony in the nucleus accumbens in vivo. J Neurosci 2001;21:4498–504.
Gray CM, Maldonado PE, Wilson M, McNaughton B. Tetrodes markedly improve the reliability and yield of multiple single-unit isolation from multi-unit recordings in cat striate cortex. J Neurosci Methods 1995;63:43–54.
Gray CM, Singer W. Stimulus-specific neuronal oscillations in orientation columns of cat visual cortex. Proc Natl Acad Sci USA 1989;86:1698–702.
Grover FS, Buchwald JS. Correlation of cell size with amplitude of background fast activity in specific brain nuclei. J Neurophysiol 1970;33:160–71.
Halliday DM, Conway BA, Farmer SF, Shahani U, Russell AJC, Rosenberg JR. Coherence between low-frequency activation of the motor cortex and tremor in patients with essential tremor. Lancet 2000;355:1149–53.
Hasenstaub A, Sachdev RN, McCormick DA. State changes rapidly modulate cortical neuronal responsiveness. J Neurosci 2007;27:9607–22.
Henze DA, Borhegyi Z, Csicsvari J, Mamiya A, Harris KD, Buzsaki G. Intracellular features predicted by extracellular recordings in the hippocampus in vivo. J Neurophysiol 2000;84:390–400.
Horwitz B. The elusive concept of brain connectivity. NeuroImage 2003;19:466–70.
Huang CM, Buchwald JS. Interpretation of the vertex short-latency acoustic response: a study of single neurons in the brain stem. Brain Res 1977;137:291–303.
Hurtado JM, Rubchinsky LL, Sigvardt KA. Statistical method for detection of phase-locking episodes in neural oscillations. J Neurophysiol 2004;91:1883–98.
Hurtado JM, Rubchinsky LL, Sigvardt KA, Wheelock VL, Pappas CT. Temporal evolution of oscillations and synchrony in GPi/muscle pairs in Parkinson's disease. J Neurophysiol 2005;93:1569–84.
Hutchison WD, Dostrovsky JO, Walters JR, Courtemanche R, Boraud T, Goldberg J, et al. Neuronal oscillations in the basal ganglia and movement disorders: evidence from whole animal and human recordings. J Neurosci 2004;24:9240–3.
Juergens E, Guettler A, Eckhorn R. Visual stimulation elicits locked and induced gamma oscillations in monkey intracortical- and EEG-potentials, but not in human EEG. Exp Brain Res 1999;129:247–59.
Legatt AD, Arezzo J, Vaughan Jr HG. Averaged multiple unit activity as an estimate of phasic changes in local neuronal activity: effects of volume-conducted potentials. J Neurosci Methods 1980;2:203–17.
Lemon RN. Methods for neuronal recording in conscious animals. New York: Wiley; 1984.
Lenz FA, Tasker RR, Kwan HC, Schnider S, Kwong R, Murayama Y, et al. Single unit analysis of the human ventral thalamic nuclear group: correlation of thalamic "tremor cells" with the 3–6 Hz component of parkinsonian tremor. J Neurosci 1988;8:754–64.
Levy R, Ashby P, Hutchison WD, Lang AE, Lozano AM, Dostrovsky JO. Dependence of subthalamic nucleus oscillations on movement and dopamine in Parkinson's disease. Brain 2002;125:1196–209.
Logothetis NK. The neural basis of the blood-oxygen-level-dependent functional magnetic resonance imaging signal. Philos Trans R Soc Lond B Biol Sci 2002;357:1003–37.
Logothetis NK. The underpinnings of the BOLD functional magnetic resonance imaging signal. J Neurosci 2003;23:3963–71.
Mitzdorf U. Current source-density method and application in cat cerebral cortex: investigation of evoked potentials and EEG phenomena. Physiol Rev 1985;65:37–100.
Mitzdorf U. Properties of the evoked potential generators: current source-density analysis of visually evoked potentials in the cat cortex. Int J Neurosci 1987;33:33–59.
Moran A, Bergman H, Israel Z, Bar-Gad I. Subthalamic nucleus functional organization revealed by parkinsonian neuronal oscillations and synchrony. Brain 2008;131:3395–409.
Murthy VN, Fetz EE. Oscillatory activity in sensorimotor cortex of awake monkeys: synchronization of local field potentials and relation to behavior. J Neurophysiol 1996;76:3949–67.
Pedemonte M, Barrenechea C, Nuñez A, Gambini JP, García-Austt E. Membrane and circuit properties of lateral septum neurons: relationships with hippocampal rhythms. Brain Res 1998;800:145–53.
Pfurtscheller G, Andrew C. Event-related changes of band power and coherence: methodology and interpretation. J Clin Neurophysiol 1999;16:512–9.
Rall W. Electrophysiology of a dendritic neuron model. Biophys J 1962;2:145–67.
Rasch MJ, Gretton A, Murayama Y, Maass W, Logothetis NK. Inferring spike trains from local field potentials. J Neurophysiol 2008;99:1461–76.
Rieke F, Warland D, de Reuter van Steveninck R, Bialek W. Spikes: exploring the neural code. Cambridge: MIT Press; 1997.

Robinson DA. The electrical properties of metal microelectrodes. Proc IEEE 1968;56:1065–71.
Rosenberg JR, Amjad AM, Breeze P, Brillinger DR, Halliday DM. The Fourier approach to the identification of functional coupling between neuronal spike trains. Prog Biophys Mol Biol 1989;53:1–31.
Schwartz AB. Cortical neural prosthetics. Annu Rev Neurosci 2004;27:487–507.
Stroeve S, Gielen S. Correlation between uncoupled conductance-based integrate-and-fire neurons due to common and synchronous presynaptic firing. Neural Comput 2001;13:2005–29.
Zeitler M, Fries P, Gielen S. Assessing neuronal coherence with single-unit, multi-unit, and local field potentials. Neural Comput 2006;18:2256–81.